

---

# TRANSFORMER WITH SELECTIVE SHUFFLED POSITION EMBEDDING USING ROI-EXCHANGE STRATEGY FOR EARLY DETECTION OF KNEE OSTEOARTHRITIS

---

**Zhe Wang**

IDP Laboratory, UMR CNRS 7013  
University of Orleans  
Orleans, France  
zhe.wang@etu.univ-orleans.fr

**Aladine Chetouani**

PRISME Laboratory, EA 4229  
University of Orleans  
Orleans, France  
aladine.chetouani@univ-orleans.fr

**Rachid Jennane**

IDP Laboratory, UMR CNRS 7013  
University of Orleans  
Orleans, France  
rachid.jennane@univ-orleans.fr

April 18, 2023

## ABSTRACT

Knee OsteoArthritis (KOA) is a prevalent musculoskeletal disorder that causes decreased mobility in seniors. The lack of sufficient data in the medical field is always a challenge for training a learning model due to the high cost of labelling. At present, deep neural network training strongly depends on data augmentation to improve the model's generalization capability and avoid over-fitting. However, existing data augmentation operations, such as rotation, gamma correction, etc., are designed based on the data itself, which does not substantially increase the data diversity. In this paper, we proposed a novel approach based on the Vision Transformer (ViT) model with Selective Shuffled Position Embedding (SSPE) and a ROI-exchange strategy to obtain different input sequences as a method of data augmentation for early detection of KOA (KL-0 vs KL-2). More specifically, we fixed and shuffled the position embedding of ROI and non-ROI patches, respectively. Then, for the input image, we randomly selected other images from the training set to exchange their ROI patches and thus obtained different input sequences. Finally, a hybrid loss function was derived using different loss functions with optimized weights. Experimental results show that our proposed approach is a valid method of data augmentation as it can significantly improve the model's classification performance.

**Keywords** Vision transformer · Position embedding · Hybrid loss · Knee osteoarthritis · Data augmentation

## 1 Introduction

Knee OsteoArthritis (KOA) is a common degenerative joint disease caused by an inflammatory response in the joint due to cartilage degeneration and damage [1]. The main symptoms of KOA include pain, swelling, stiffness and impaired movement. Patients usually feel pain around the knee joint, which becomes worse over time and can even persist at rest. Swelling is due to an inflammatory response, while stiffness is due to a reduction in cartilage and restricted movement of the joint due to arthritic lesions. KOA is usually caused by a number of factors including genetics, age, obesity, joint damage, and lifestyle [2]. Current treatments for KOA include medication, physiotherapy, and surgery [3]. Medication can relieve symptoms by reducing pain and inflammation, while physiotherapy can strengthen muscles and reduce stress through exercise, massage, and physical therapy. In severe cases, surgical treatment is necessary, such as joint replacement surgery [4].

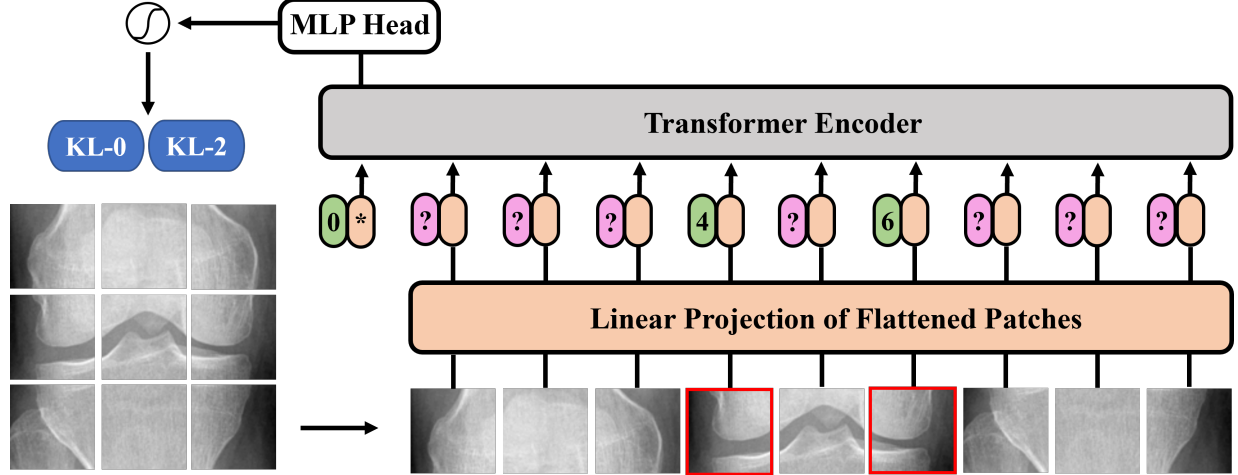


Figure 1: The flowchart of the proposed approach. Black arrows show the data-flow. Green and purple blocks represent the fixed and shuffled position embeddings, respectively.

The Kellgren-Lawrence (KL) grading system [5] was proposed in 1957 as a gold standard in the assessment of KOA when using plain radiographs. KOA severity can be defined into five grades depending on the existence and degree of symptoms: KL-0 indicates a definite absence of osteoarthritis; KL-1 suggests possible osteophytic lipping; KL-2 represents definite osteophytes and possible joint space narrowing (JSN); KL-3 indicates definite JSN, some sclerosis, and possible deformity of bone ends; and KL-4 denotes large osteophytes, definite JSN, severe sclerosis, and definite deformity of bone ends. However, the diagnosis of KOA relies completely on the perception and judgement of each medical professional, with practitioners potentially differing in their assessments for the same knee X-ray image [6].

Computer hardware advancements have enabled deep learning to play a greater role in Computer Vision (CV). All the time, Convolutional Neural Networks (CNNs) [7] have been able to effectively execute tasks such as detection [8], segmentation [9] and classification [10]. In recent years, with the successful application of Transformers in Natural Language Processing (NLP), the Transformer-based model, namely Vision Transformer (ViT), have also shown the ability to compete with CNN in CV.

Several CNN-based and ViT-based learning models have been proposed for KOA diagnosis in the literature. In [11], Antony et al. employed the Fully Convolutional Neural (FCN) network [12] to locate the knee joint automatically and classify full KL grades using the classical CNN. In [13], Tiuplin et al. cropped two patches from the lateral and medial parts of the knee joint X-ray images as the input pair of the Siamese network to evaluate the KOA grade. In [14], Alshareef et al. used the ViT-L32 model to classify knee osteoarthritis with an accuracy of 1.48% higher than that of the classical CNN approach.

In the realm of deep learning for CV, particularly in the medical imagery, the scarcity of high-quality medical dataset poses a significant challenge for training deep learning models due to the costly labelling process [15]. To tackle this problem, deep neural networks rely heavily on data augmentation techniques to enhance the model’s generalization capability and prevent over-fitting [16]. However, conventional augmentation methods, such as rotation and gamma correction, do not fundamentally change the data structure of the samples, resulting in limited sample diversity. To address this issue, we drew inspiration from [17] and [18] and introduced the concept of data augmentation within and outside the model, respectively.

It is noteworthy that KOA is definitely present at KL-2, although of minimal severity. Patients at advanced stages of KOA (KL-3 and KL-4) usually have recourse to total knee replacement [19]. Hence, early detection of KOA is clinically more worthwhile and is thus the objective of this study. However, since the label data for KL-1 patients are often regarded as doubtful in the literature, they may contain high uncertainties that could lead to unstable model training and inaccurate prediction results. Therefore, in this study, we focused solely on KL-0 and KL-2 as the early detection of KOA. To do this, we proposed an approach combining the ViT-based learning model, a ROI-exchange strategy and a hybrid loss for the early detection of KOA (KL-0 vs KL-2). More specifically, we used ViT-base-patch16-224-in21k as a pre-trained model. Then, we forced the model to focus only on the patches associated with symptoms of KL-2 applying the Selective Shuffled Position Embedding (SSPE), which can be considered as a data augmentation within the model. Moreover, we exchanged the ROIs from other images to conduct the new input sequences as a data augmentation

outside the model. Finally, a hybrid loss consists of Label Smoothing Cross-Entropy (LSCE) (see Eq. 5) loss and CE loss was computed with optimized weights.

The main contributions of this paper are as follows:

- A novel ViT-based learning model with well-designed position embedding is proposed.
- A ROI-exchange strategy is introduced as a method of data augmentation.
- Attention maps given by the Grad-CAM technique are provided to highlight regions that contribute to the network’s decision.
- All experiments are conducted on the publicly-available database, the OsteoArthritis Initiative (OAI) [20].

## 2 Proposed Approach

The flowchart of the proposed approach is presented in Fig. 1. The main symbols used in this paper are given in Table 1.

Table 1: Important symbols used in this paper

Symbol	Description
$\mathcal{K}$	Set of KL grades (KL-0 and KL-2)
$\mathcal{D}$	Overall dataset
$\mathcal{T}$	Training set
$\hat{Y}$	Predicted labels
$Y$	Real labels

### 2.1 Proposed learning model

Before describing the proposed approach, we briefly present the structure of the classical Transformer network, which was first introduced in a seminal paper by Vaswani et al. [21] in 2017. It is particularly well-suited to Natural Language Processing (NLP) tasks, such as language translation [22] and text classification [23]. Unlike traditional neural networks, which process input data sequentially and are therefore prone to losing information about long-term dependencies, Transformers are designed to be capable of parallel processing, making them more efficient and capable of modelling long-range dependencies [24]. The key innovation behind Transformers is the self-attention mechanism, which allows the network to selectively attend to different parts of the input sequence in order to capture the most relevant information for a given task. This mechanism has proven to be particularly effective in NLP [25], where the relationship between different words in a sentence can be complex and nuanced.

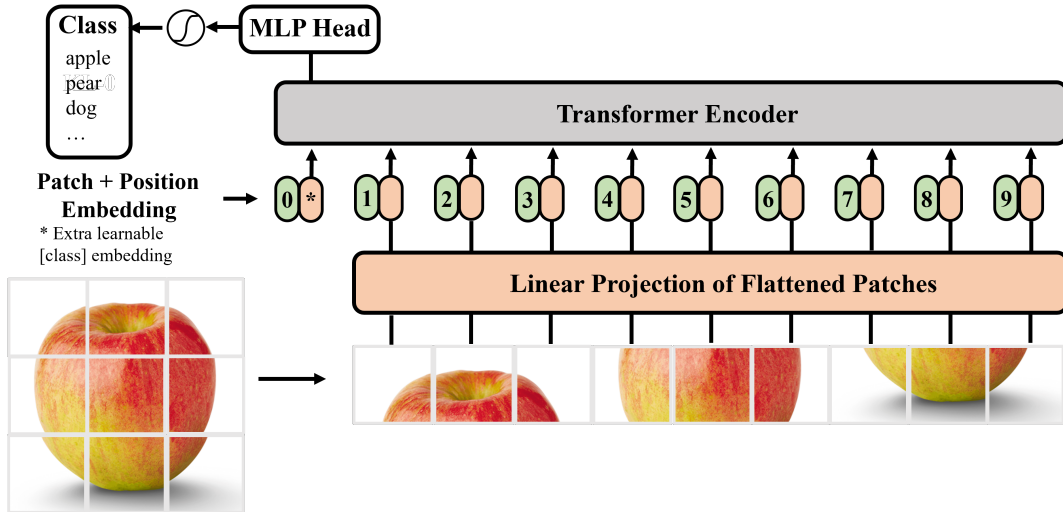


Figure 2: The structure of the classical ViT network.

Vision Transformer (ViT) is a neural network architecture introduced in a paper by Dosovitskiy et al. [26] in 2020. It represents a breakthrough in CV, as it demonstrated that Transformers, originally designed for NLP, could also be applied successfully to image-based tasks. As shown in Fig. 2, the key idea behind ViT is to treat an image as a sequence of patches rather than as a grid of pixels and to apply a Transformer network to these patches. The resulting network can then be trained using standard backpropagation techniques on a large-scale image dataset. One of the advantages of ViT over traditional CNNs is that it is capable of capturing global spatial relationships in an image [27], which is especially important for tasks such as object recognition and image classification. In addition, ViT is highly efficient since it can process an entire image in parallel, unlike CNNs, which require sequential processing. ViT has achieved state-of-the-art performance on a range of CV tasks, including image classification [28], object detection [29], and image segmentation [30]. As a result, ViT has quickly become one of the most popular architectures in CV research.

Usually, ViT uses learnable absolute positional embedding to encode different positions. For each input patch, a position encoding vector is assigned with the same dimension as the embedding vector of the Transformer. During input, the position embedding vector is added to the input vector to preserve the relative positional information between different positions. For each position  $i$  and each position encoding dimension  $j$ , the position embedding is calculated by adding a sine encoding and a cosine encoding:

$$PE_{i,j} = \begin{cases} \sin(\frac{i}{10000^{2j/d}}), & \text{if } j \text{ is even} \\ \cos(\frac{i}{10000^{2(j-1)/d}}), & \text{if } j \text{ is odd} \end{cases} \quad (1)$$

where  $d$  is the dimension of the position embedding, which is typically set to an even number.

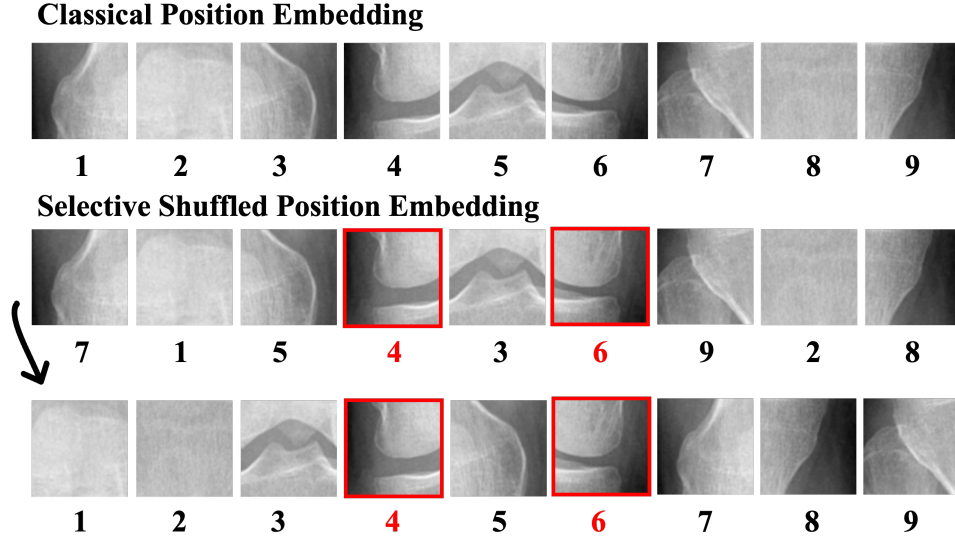


Figure 3: The classical position embedding and the proposed selective shuffled position embedding.

Considering that the symptoms of KL-2 (i.e., osteophytes and JSN) are only manifested in specific areas (patches) of the knee and inspired by the work of [17] and [18], as shown in Fig. 3, compared to the classical position embedding, we proposed a novel position embedding strategy, namely Selective Shuffled Position Embedding (SSPE). Specifically, we first fixed the position encoding of the ROI patches (i.e., red boxes in Fig. 3), then we shuffled the position encoding of the remaining patches (i.e., non-ROI patches). Finally, an input sequence of non-ROI patches in different orders is obtained. SSPE can force the ViT model to focus only on the Regions Of Interest (ROIs) related to KL-2, thus achieving a certain degree of data augmentation within the model. It is noteworthy that the position encoding for non-ROI patches is shuffled for each training epoch.

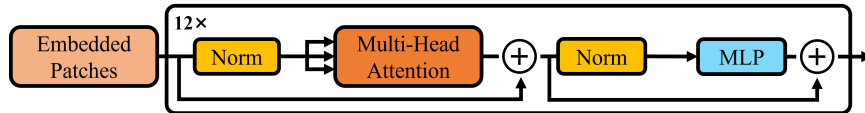


Figure 4: The structure of the encoder module.

Here, we also briefly present the encoder module of the ViT model, which consists of a stack of 12 identical Transformer blocks. As shown in Fig. 4, each Transformer block is composed of two sub-layers, namely, the multi-head self-attention layer and the Multi-Layer Perceptron (MLP). Multi-head self-attention layer is responsible for capturing the relationships between different parts of the image. It consists of multiple parallel attention heads, each of which learns to attend to different parts of the image. The outputs of these attention heads are then concatenated and linearly projected to produce the final output of the self-attention layer. MLP, also namely as the feedforward neural network layer, is responsible for transforming the features learned by the self-attention layer into a form that can be easily used by subsequent layers. It consists of two linear transformations followed by a non-linear activation function.

## 2.2 ROI-exchange strategy

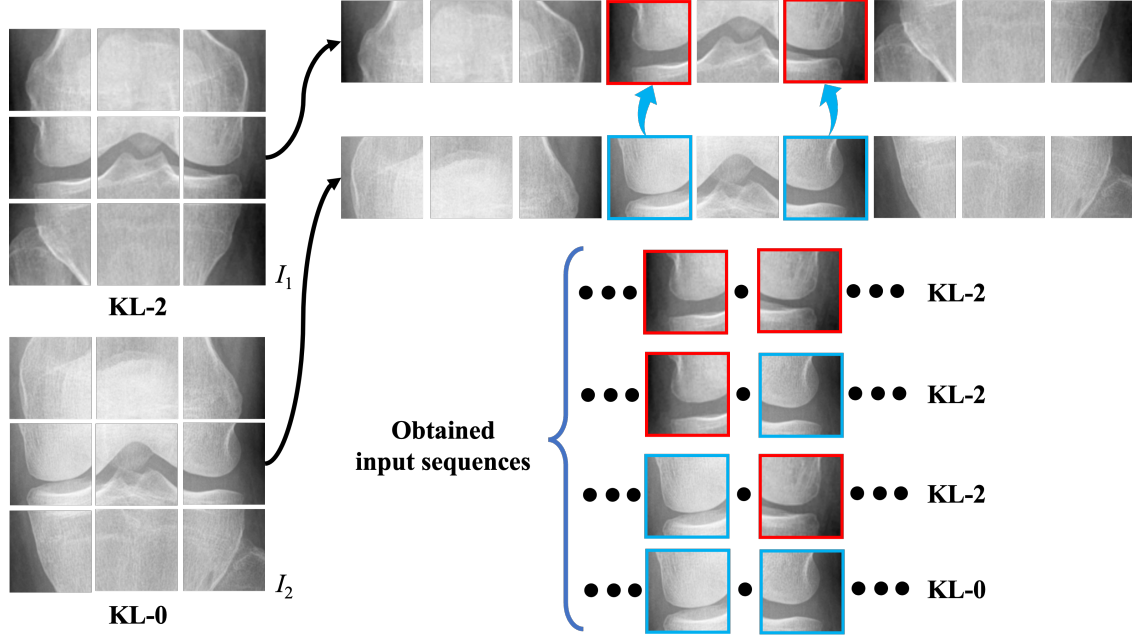


Figure 5: The proposed ROI-exchange strategy and the definition of the label for each obtained input sequences.

As explained previously, our proposed position embedding strategy aims to make the model focus on the ROI patches, which is the concept of data augmentation integrated into the model structure. Here, we also introduced a method of data augmentation outside the model. Inspired by the work of [18], we exchanged ROIs between and within the KL grades. More specifically, for any input image  $I_1$ , we randomly selected other  $N$  images  $I_2, I_3, \dots, I_{N+1}$  from the training set  $\mathcal{T}$  and exchanged their ROI patches, resulting in four different input sequences. It is worth noting that ROIs can only be exchanged according to the specific positions ( $\#4 \leftrightarrow \#4$ ;  $\#6 \leftrightarrow \#6$ ), and the non-ROI patches remain the same as those of the input image  $I_1$ . The number of match  $N$  will be discussed in Section 4.3. The labels  $l$  of resulting input sequences are defined as follows:

$$l = \begin{cases} \text{KL-0}, & \text{if } \forall i \in [1, 2], l_i = \text{KL-0} \\ \text{KL-2}, & \text{otherwise} \end{cases} \quad (2)$$

where  $l_i$  represents the label of each ROI patch.

## 2.3 Hybrid loss strategy

The proposed hybrid loss strategy is based on the use of two loss functions: LSCE and CE, for input sequences of mix-KL-ROI,  $\mathcal{M}$ , and full-KL-ROI,  $\mathcal{F}$ , respectively.

Firstly, the LSCE loss function was used for the set  $\mathcal{M}$  to avoid the learning model being overconfident. To this end, we used label smoothing [31], which is a regularization technique that consists in perturbing the target variable to make the learning model less certain of its prediction.

Label smoothing replaces the one-hot encoded label vector  $y_s^{hot}$  by a mixture of  $y_s^{hot}$ , named  $y_s^{LS}$ :

$$y_s^{LS} = y_s^{hot}(1 - \varepsilon) + \frac{\varepsilon}{2}, \quad y_s^{hot} \in \{0, 1\}, \varepsilon \in (0, 1) \quad (3)$$

$$y_s^{hot} = \begin{cases} 1 & \hat{Y} = T \\ 0 & \hat{Y} \neq T \end{cases} \quad (4)$$

where  $y_s^{hot}$  is the one-hot encoded ground-truth label of the sample  $s$ , and  $\varepsilon$  is an hyper-parameter that determines the amount of smoothing.

The LSCE loss,  $J_{LSCE}$  is thus computed as follows:

$$\begin{aligned} J_{LSCE} &= \sum_{s \in \mathcal{M}} -y_s^{LS} \log(p_s) \\ &= \sum_{s \in \mathcal{M}} -(y_s^{hot}(1 - \varepsilon) + \frac{\varepsilon}{2}) \log(p_s) \end{aligned} \quad (5)$$

$$p_s = P_{\hat{Y}|T}(\hat{Y} = k | T = k), \quad \forall k \in \mathcal{K}, \forall s \in \mathcal{D} \quad (6)$$

where  $\hat{Y}$  and  $T$  are the predicted and the real labels, respectively,  $k$  represents the KL grade of the sample  $s$ ,  $P_{\hat{Y}|T}$  is the conditional probability distribution,  $\mathcal{K}$  is a set of KL grades (KL-0 and KL-2), and  $\mathcal{D}$  is the overall dataset.

Secondly, for input sequences of full-KL-ROI, set  $\mathcal{F}$ , the classical CE loss,  $J_{CE}$  was used and computed as follows:

$$J_{CE} = \sum_{s \in \mathcal{F}_k} -y_s^{hot} \log(p_s), \quad \forall k \in \mathcal{K}, \forall s \in \mathcal{F} \quad (7)$$

Finally, the proposed hybrid loss function was defined as follows:

$$J_{hybrid} = \alpha J_{LSCE} + \beta J_{CE} \quad (8)$$

where the hyper-parameters  $\alpha$  and  $\beta$  were used to weight and better balance the considered loss functions, which will be discussed in Section 4.2.

### 3 Experiments

In this section, experimental data and details are presented.

#### 3.1 Public knee database

We used knee X-rays from the Osteoarthritis Initiative (OAI) [20], which is publicly available. The OAI is a longitudinal study of 4796 individuals aged between 45 to 79 years of age followed over 96 months, with each participant having nine follow-up examinations. The aim of the OAI study was to observe participants who already suffered from KOA or from an elevated risk of developing it. All the collected data are publicly available to accelerate research in the field of KOA.

#### 3.2 Data preprocessing

As shown in Fig. 6, lateral and medial patches of the knee joint were the foci of this study to enable early KOA detection. More specifically, knee joints, as in [32], were detected using YOLOv2 [33] and served as inputs of the proposed model. As a result of the preprocessing steps, 3,185 KL-0 and 2,126 KL-2 images were collected. According to each KL grade, the dataset was randomly divided into training, validation, and test sets with a ratio of 7:1:2, respectively.



Figure 6: (a) An original knee radiograph from OAI and a detected knee joint in red box. (b) An obtained knee joint.

### 3.3 Experimental details

We used the pre-trained weights of the model ViT-base-patch16-224-in21k. The Adam optimizer [34] was applied to train 100 epochs with a learning rate of  $5e-06$  and a batch of size 128. Data augmentation [35] was executed randomly including random rotation, brightness, contrast, jitter, and gamma correction. To deal with the imbalanced dataset of the study, bootstrapping-based oversampling [36] was applied. To avoid over-fitting, weight decay [37] was parameterized at a coefficient of  $3e-04$  and dropout [38] at 0.2. Our approach was implemented using PyTorch v1.8.1 [39] on Nvidia TESLA A100 with 80 GB memory graphic cards.

## 4 Results and discussion

In this section, experimental results are presented and discussed. KL-2 was treated as the positive class to compute the F1-score.

### 4.1 Comparison of position embedding

For greater convenience and a fair comparison, we only used here the original input sequences without the ROI-exchange strategy. As shown in Table 2, an ablation study on different embedding methods and proposed SSPE strategy were achieved. More specifically, for different embedding methods:

- 1-D position embedding: The classical position embedding is calculated as Eq.1 in Section 2.1.
- 2-D position embedding: Each pixel or location in an image is represented as a vector that encodes both the row and column positions of the pixel.
- Relative position embedding: It encodes the position of each token relative to all the other tokens in the sequence.

Table 2: Comparison of position embedding

Position Embedding	Acc (%)		Acc (%)	Diff (%)
No Pos. Emb.	85.12	with SSPE	-	-
1-D Pos. Emb.	<b>88.44</b>		<b>88.86</b>	0.42 ↑
2-D Pos. Emb.	87.81		88.29	<b>0.48</b> ↑
Rel. Pos. Emb.	87.69		87.99	0.30 ↑

As can be seen, regardless of which position embedding method is used, our proposed SSPE strategy can always improve the performance of the model, as it increases the diversity of the input data (sequences) to some extent changing the data structure, which achieved the purpose of data augmentation from within the model.

## 4.2 Selection of the hyper-parameters

To show the impact of the hyper-parameters (i.e.,  $\varepsilon$ ,  $\alpha$ , and  $\beta$ ) of the proposed hybrid loss function for the ROI-exchange strategy, different configurations were tested with  $N = 1$ . We first determined the level of smoothing  $\varepsilon \in [0.05, 0.3]$ . Then, we evaluated the weight hyper-parameters through a small grid search over combinations of  $\alpha, \beta \in [0.1, 1]$  ensuring that  $\alpha + \beta = 1$ . For greater convenience, here we only show the performance obtained for each  $\varepsilon$  with the most optimized weight parameters  $\alpha$  and  $\beta$ . Several conclusions can be drawn from the Table 3. Firstly, using the ROI-exchange strategy generally improves the accuracy of the model. Secondly, while using the hybrid loss strategy during training may not always improve accuracy, it can be effective depending on the values of hyper-parameters  $\varepsilon$ ,  $\alpha$ , and  $\beta$ . The highest accuracy of 89.80% was achieved with  $\varepsilon = 0.2$ ,  $\alpha = 0.3$ , and  $\beta = 0.7$ , indicating the importance of careful selection of hyper-parameters in achieving optimal performance.

Table 3: Contribution of different combinations of hyper-parameters

	$\varepsilon$	$\alpha$	$\beta$	Acc (%)	Diff <sub>1</sub> <sup>1</sup> (%)	Diff <sub>2</sub> <sup>2</sup> (%)
with ROI-exchange strategy	without hybrid loss <sup>3</sup>					
	-	0	1	89.32	0.46 ↑	-
	with hybrid loss					
	0.05	0.2	0.8	89.11	0.25 ↑	0.21 ↓
	0.10	0.4	0.6	89.29	0.43 ↑	0.03 ↓
	0.15	0.3	0.7	89.57	0.71 ↑	0.25 ↑
	0.20	0.3	0.7	<b>89.80</b>	<b>0.94</b> ↑	<b>0.48</b> ↑
	0.25	0.4	0.6	88.96	0.10 ↑	0.36 ↓
	0.30	0.5	0.5	88.91	0.05 ↑	0.41 ↓

<sup>1</sup> Diff<sub>1</sub>: The accuracy difference compared to the model using SSPE without ROI-exchange strategy.

<sup>2</sup> Diff<sub>2</sub>: The accuracy difference compared to the model using SSPE without hybrid loss.

<sup>3</sup> Only classical CE loss was used.

## 4.3 Effects of the number of match

As presented in Section 2.1, we randomly selected other  $N$  images,  $I_2, I_3 \dots I_{N+1}$ , to match the initial input image  $I_1$  to exchange the ROI patches. Here, we evaluated the contribution of  $N \in [1, 5]$  to the model performance in terms of the speed of convergence and accuracy. As can be seen, Fig. 7(a) displays that as  $N$  increases, the convergence of the model slows down and the final training loss generally decreases. Nevertheless, after  $N = 2$ , the gains from increasing  $N$  become less pronounced. Fig. 7(b) shows the corresponding classification accuracy of the model for varying values of  $N$ . The accuracy demonstrates a positive correlation with the number of matches between 1 and 3. However, setting  $N$  to a higher value (e.g.,  $N = 5$ ) decreases accuracy, although it remains better than the initial accuracy. Considering the trade-off between effect and computational efficiency, we ultimately opted for  $N = 2$  as the optimal number of match for the ROI-exchange strategy.

## 4.4 Comparison with different learning models

In this section, our proposed approach is compared to existing deep learning-based models. Results are shown in Table 4 in terms of accuracy, F1-score and the number of parameters. As can be seen, our proposed approach outperforms all the evaluated ones in terms of accuracy and F1-score, which shows that our proposed global approach: SSPE and ROI-exchange strategies can effectively improve the model’s performance, as they both perform data augmentation on the input sequences. However, the shortcoming is the relatively high number of parameters in our model, especially compared to the works of [13] and [17], which will be discussed in Section 4.7.

To visualise the regions that contributed to the decision of each model, the Grad-Cam technique [40] was used. The attention maps thus obtained are presented in Fig. 8. As can be noticed, all evaluated models show a certain sensitivity to regions that involve early KOA (KL-2) characteristics (i.e., osteophytes and JSN). However, models from DenseNet, ResNet, and VGG series also exhibit a reaction to background noise, which may negatively impact their classification performance. Conversely, our proposed approach and the Siamese-based models (i.e., [13] and [17]) focus more on regions affected by KOA, which demonstrates that with a well-designed position embedding layer, we can make the model concentrate on specific areas where the effectiveness of attention areas is as good as that of Siamese-based



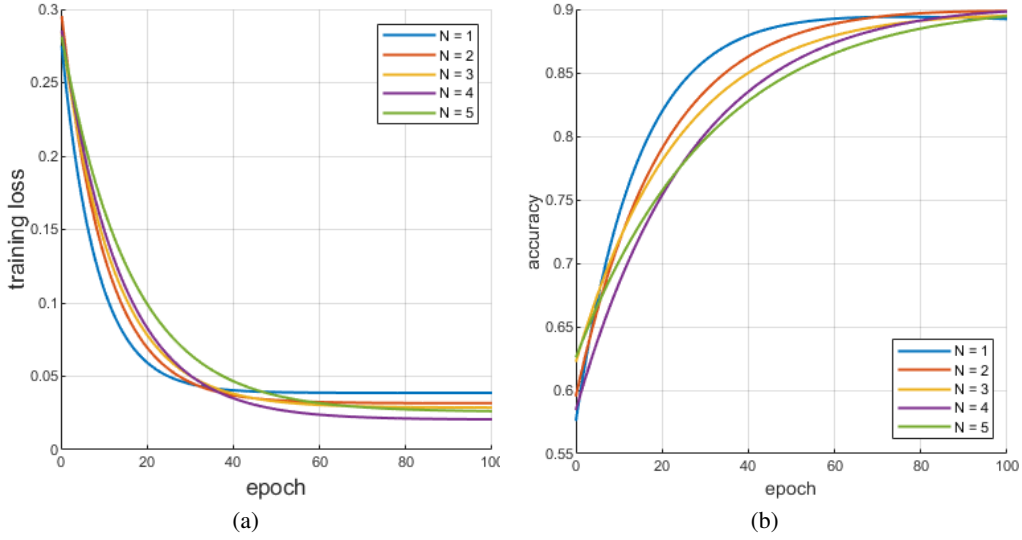


Figure 7: Training loss (a) and accuracy (b) curves obtained within 100 epochs using different numbers of match,  $N$ .

Table 4: Comparison of the performance of different models

Models	Accuracy (%)	F1 (%)	Params ( $M$ ) <sup>1</sup>
Densenet-121	80.84	77.03	6.95
Densenet-161	79.06	75.09	26.47
Densenet-169	81.81	78.23	12.48
Densenet-201	84.43	81.29	18.09
Resnet-18	83.59	80.30	11.17
Resnet-34	80.14	76.35	21.28
Resnet-50	81.78	78.29	23.51
Resnet-101	77.60	72.98	42.50
Resnet-152	76.47	72.13	58.14
VGG-11	80.97	77.30	195.89
VGG-13	80.71	77.88	196.07
VGG-16	73.17	68.50	201.38
VGG-19	71.98	68.84	206.70
Tiuplin et al. [13]	87.33	84.82	<b>0.15</b>
Wang et al. [17]	88.38	85.93	2.71
Our model	<b>89.80</b>	<b>87.66</b>	85.95

<sup>1</sup> Params is the number of parameters used by the model

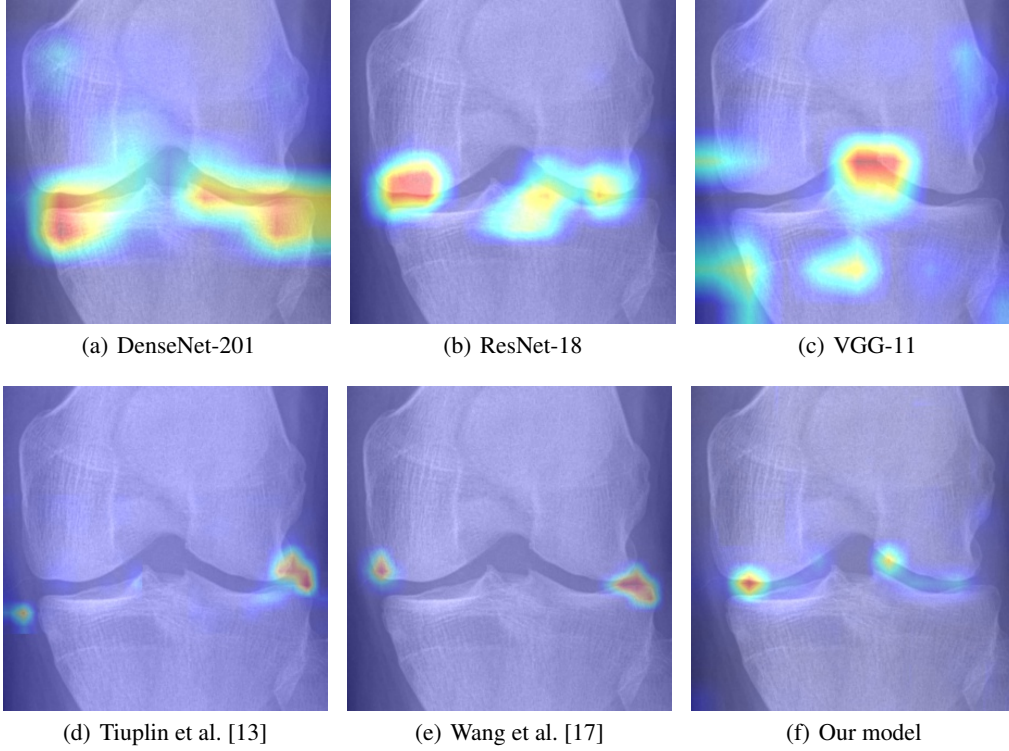


Figure 8: Comparison of attention maps obtained from the last layer using different learning models.

models. However, compared to our method, the Siamese-based network requires users to manually crop the ROIs during the data pre-processing, making it less fully automatic. Additionally, thanks to the ordered position embedding of ROI patches, our model can better handle their sequential information. As can be seen, the attention areas of our model were extended well between the joint space rather than just on the position of osteophytes, which maintains a higher degree of consistency with the behaviour of medical professionals diagnosing KOA.

#### 4.5 Contribution of the hybrid loss

As presented in Section 2.3, our proposed hybrid loss combines the CE loss and the LSCE loss, which were applied to the full-KL-ROI,  $\mathcal{F}$ , and the mix-KL-ROI,  $\mathcal{M}$  sequences, respectively. Here, we presented the contribution of the proposed hybrid loss with the most optimised hyper-parameters discussed in Section 4.2 visualising the t-SNE scatter plot. As shown in Fig. 9, compared with a single CE loss function, our proposed hybrid loss strategy ensures consistent inter-class distance (i.e., centre points of two classes) and makes the distribution of samples of each class more continuous by appropriately increasing intra-class distance, which is consistent with the objective continuity of KL grades, which to some extent alleviates the problem of overconfidence in model training caused by the semi-quantitative nature of the KL grading system.

#### 4.6 Analysis of the applicability

In this section, we analyzed the applicability of our proposed global approach on the common pre-trained ViT models. Table 5 presents the performance achieved using all proposed strategies (i.e., SSPE, ROI-exchange, and hybrid loss). Here, in the hybrid loss strategy, the same hyper-parameters that obtained the best performance were used for a fair comparison. As can be seen, our proposed global approach consistently improves accuracy across all ViT series models, indicating its broad applicability.

#### 4.7 Discussion

In this paper, we have introduced a novel approach for the early detection of KOA (KL-0 vs KL-2) based on the ViT network. Firstly, we fixed and shuffled the position encoding of the ROI and non-ROI patches in the input sequences,

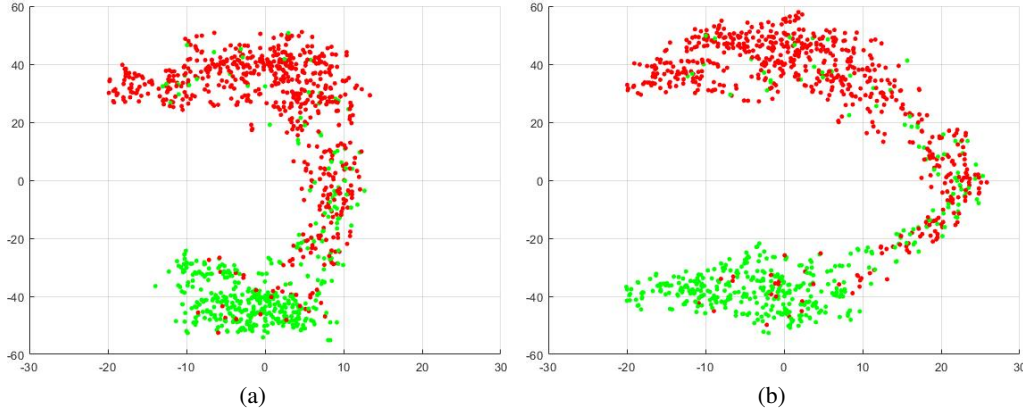


Figure 9: t-SNE scatter plots obtained using the CE loss (a) and the proposed hybrid loss (b).

Table 5: Applicability of the proposed global approach

Pre-trained model	Acc (%)	Acc <sup>*1</sup> (%)	Diff (%)	Param ( $M$ )
ViT-base-patch16-224	88.31	89.11	0.80 $\uparrow$	<b>85.95</b>
ViT-base-patch16-224-in21k <sup>2</sup>	88.44	89.80	<b>1.36</b> $\uparrow$	<b>85.95</b>
ViT-base-patch32-224	88.39	89.29	0.90 $\uparrow$	87.50
ViT-base-patch32-224-in21k	88.52	89.69	1.17 $\uparrow$	87.50
ViT-large-patch16-224	88.52	89.71	1.19 $\uparrow$	303.51
ViT-large-patch16-224-in21k	88.61	<b>89.84</b>	1.23 $\uparrow$	303.51
ViT-large-patch32-224-in21k	<b>88.73</b>	89.82	1.09 $\uparrow$	305.56

<sup>1</sup> Acc\*: Accuracy obtained using our proposed global approach.<sup>2</sup> The pre-trained model used in this study.

respectively, to achieve data augmentation within the model. Then, we randomly selected other  $N$  images for the input image to exchange their ROIs to obtain different input sequences, which achieves data augmentation outside the model. Finally, an adequate hybrid loss strategy was proposed, which consists of the combination of the CE loss and the LSCE loss. These two loss functions were optimised adjusting the weights  $\alpha$  and  $\beta$ . Our experimental findings demonstrated the validity of our proposed global approach, as it can significantly improve the model’s classification performance.

#### 4.7.1 Details of the position embedding

As presented in Section 2.1, the position embedding layer was used to capture the spatial information of each pixel or feature map. To make the model focus only on the ROI patches, we proposed SSPE to diversify the input sequences and simultaneously used the dropout technique. More specifically, we evaluated several random dropouts of 20%, 30%, and 50% to the position encoding of non-ROI patches for the classic position embedding and SSPE, respectively. However, no improvement was observed, which is probably caused by the fact that the diversity of the input sequences decreases when we randomly drop the positional information of non-ROI patches.

#### 4.7.2 Strengths and limitations

This study has several notable strengths. From a clinical perspective, focusing on early KOA diagnosis (KL-0 vs KL-2) is particularly relevant as it enables timely physical interventions that can potentially delay the onset and progression of KOA symptoms. To ensure the clinical applicability of our model, we undertook several steps: First, we fixed the position encoding of ROI patches, which is consistent with the attention areas that radiologists consider when diagnosing KOA [41]. Secondly, during our ROI-exchange strategy, all sequences obtained are composed of patches from real and valid data. Finally, common data augmentation techniques such as rotation, gamma correction, and jitter were also used to further enhance the stability and robustness of the model. We believe that such a more stable and explainable model in a Computer-Aided Diagnosis (CAD) system can make deep learning approaches gain more trust and acceptance from medical practitioners in daily clinical practice. There were also several limitations in our study. All experiments were only achieved using the OAI database. Other large databases should be considered to evaluate and

strengthen the proposed approach. Moreover, as presented in Table 4, although our approach’s accuracy is higher than that of Siamese-based models (i.e., [13] and [17]), the high computational cost is still a major impediment to clinical applications, given its high reliance on high-end hardware. Therefore, the use of other large datasets such as Multicenter Osteoarthritis Study (MOST) and continued optimisation of the baseline model for specific tasks could be of interest for future work.

## 5 Acknowledgements

The authors would like to express their gratitude to the French National Research Agency (ANR) for supporting their work through the ANR-20-CE45-0013-01 project.

This manuscript was prepared using OAI data and does not necessarily reflect the opinions or views of the OAI investigators, the NIH, or the private funding partners. The authors would like to thank studies participants and clinical staff as well as the coordinating centre at UCSF.

## References

- [1] Richard F Loeser, Steven R Goldring, Carla R Scanzello, and Mary B Goldring. Osteoarthritis: a disease of the joint as an organ. *Arthritis and rheumatism*, 64(6):1697, 2012.
- [2] Anna Litwic, Mark H. Edwards, Elaine M. Dennison, and Cyrus Cooper. Epidemiology and burden of osteoarthritis. *British Medical Bulletin*, 105(1):185–199, 01 2013.
- [3] Wei Boon Lim and Oday Al-Dadah. Conservative treatment of knee osteoarthritis: A review of the literature. *World Journal of Orthopedics*, 13(3):212, 2022.
- [4] Jean-Pierre Raynauld, Johanne Martel-Pelletier, Marc Dorais, Boulos Haraoui, Denis Choquette, François Abram, André Beaulieu, Louis Bessette, Frédéric Morin, Lukas M Wildi, et al. Total knee replacement as a knee osteoarthritis outcome: predictors derived from a 4-year long-term observation following a randomized clinical trial using chondroitin sulfate. *Cartilage*, 4(3):219–226, 2013.
- [5] J. H. Kellgren and J. S. Lawrence. Radiological Assessment of Osteo-Arthrosis. *Annals of the Rheumatic Diseases*, 16(4):494, 1957.
- [6] Lior Shamir, Shari M Ling, William W Scott, Angelo Bos, Nikita Orlov, Tomasz J Macura, D Mark Eckley, Luigi Ferrucci, and Ilya G Goldberg. Knee x-ray image analysis method for automated detection of osteoarthritis. *IEEE Transactions on Biomedical Engineering*, 56(2):407–415, 2008.
- [7] A. Krizhevsky, I. Sutskever, and G. E Hinton. Imagenet classification with deep convolutional neural networks. *Advances in neural information processing systems*, 25:1097–1105, 2012.
- [8] Philipp V Rouast and Marc TP Adam. Learning deep representations for video-based intake gesture detection. *IEEE journal of biomedical and health informatics*, 24(6):1727–1737, 2019.
- [9] Qiaokang Liang, Yang Nan, Gianmarc Coppola, Kunglin Zou, Wei Sun, Dan Zhang, Yaonan Wang, and Guanzhen Yu. Weakly supervised biomedical image segmentation by reiterative learning. *IEEE Journal of Biomedical and Health Informatics*, 23(3):1205–1214, 2019.
- [10] Serap Aydın. Deep learning classification of neuro-emotional phase domain complexity levels induced by affective video film clips. *IEEE Journal of Biomedical and Health Informatics*, 24(6):1695–1702, 2020.
- [11] J. Antony, K. McGuinness, K. Moran, and N. E O’Connor. Automatic detection of knee joints and quantification of knee osteoarthritis severity using convolutional neural networks. In *International conference on machine learning and data mining in pattern recognition*, pages 376–390. Springer, 2017.
- [12] J. Long, E. Shelhamer, and T. Darrell. Fully convolutional networks for semantic segmentation. In *Proceedings of the IEEE conference on computer vision and pattern recognition*, pages 3431–3440, 2015.
- [13] A. Tiulpin, J. Thevenot, E. Rahtu, P. Lehenkari, and S. Saarakkala. Automatic knee osteoarthritis diagnosis from plain radiographs: A deep learning-based approach. *Scientific Reports*, 2018.
- [14] Esam Alsadiq Alshareef, Fawzi Omar Ebrahim, Yosra Lamami, Mohamed Burid Milad, Mohamed SA Eswani, Sedigh Abdalla Bashir, Salah AM Bshina, Anas Jakdoum, Asharaf Abourqeeqah, Mohamed O Elbasir, et al. Knee osteoarthritis severity grading using vision transformer. *Journal of Intelligent & Fuzzy Systems*, (Preprint):1–11, 2022.

- [15] Julia Röglin, Katharina Ziegeler, Jana Kube, Franziska König, Kay-Geert Hermann, and Steffen Ortmann. Improving classification results on a small medical dataset using a gan; an outlook for dealing with rare disease datasets. *Frontiers in Computer Science*, page 102, 2022.
- [16] Connor Shorten and Taghi M Khoshgoftaar. A survey on image data augmentation for deep learning. *Journal of big data*, 6(1):1–48, 2019.
- [17] Zhe Wang, Aladine Chetouani, Didier Hans, Eric Lespessailles, and Rachid Jennane. Siamese-gap network for early detection of knee osteoarthritis. In *2022 IEEE 19th International Symposium on Biomedical Imaging (ISBI)*, pages 1–4, 2022.
- [18] Zhe Wang, Aladine Chetouani, and Rachid Jennane. Key-exchange convolutional auto-encoder for data augmentation in early knee osteoarthritis classification. *arXiv preprint arXiv:2302.13336*, 2023.
- [19] J. A. D. van der Woude, S. C. Nair, R. J. H. Custers, J. M. van Laar, N. O. Kuchuck, F. P. J. G. Lafeber, and P. M. J. Welsing. Knee joint distraction compared to total knee arthroplasty for treatment of end stage osteoarthritis: Simulating long-term outcomes and cost-effectiveness. *PLOS ONE*, 11(5):1–13, 05 2016.
- [20] G. Lester. The Osteoarthritis Initiative: A NIH Public–Private Partnership. *HSS Journal: The Musculoskeletal Journal of Hospital for Special Surgery*, 8(1):62–63, 2011.
- [21] Ashish Vaswani, Noam Shazeer, Niki Parmar, Jakob Uszkoreit, Llion Jones, Aidan N Gomez, Łukasz Kaiser, and Illia Polosukhin. Attention is all you need. *Advances in neural information processing systems*, 30, 2017.
- [22] Mattia A Di Gangi, Matteo Negri, and Marco Turchi. Adapting transformer to end-to-end spoken language translation. In *Proceedings of INTERSPEECH 2019*, pages 1133–1137. International Speech Communication Association (ISCA), 2019.
- [23] Zein Shaheen, Gerhard Wohlgenannt, and Erwin Filtz. Large scale legal text classification using transformer models. *arXiv preprint arXiv:2010.12871*, 2020.
- [24] Salman Khan, Muzammal Naseer, Munawar Hayat, Syed Waqas Zamir, Fahad Shahbaz Khan, and Mubarak Shah. Transformers in vision: A survey. *ACM computing surveys (CSUR)*, 54(10s):1–41, 2022.
- [25] Rami Al-Rfou, Dokook Choe, Noah Constant, Mandy Guo, and Llion Jones. Character-level language modeling with deeper self-attention. In *Proceedings of the AAAI conference on artificial intelligence*, volume 33, pages 3159–3166, 2019.
- [26] Alexey Dosovitskiy, Lucas Beyer, Alexander Kolesnikov, Dirk Weissenborn, Xiaohua Zhai, Thomas Unterthiner, Mostafa Dehghani, Matthias Minderer, Georg Heigold, Sylvain Gelly, et al. An image is worth 16x16 words: Transformers for image recognition at scale. *arXiv preprint arXiv:2010.11929*, 2020.
- [27] Kai Han, Yunhe Wang, Hanling Chen, Xinghao Chen, Jianyuan Guo, Zhenhua Liu, Yehui Tang, An Xiao, Chunjing Xu, Yixing Xu, et al. A survey on vision transformer. *IEEE transactions on pattern analysis and machine intelligence*, 45(1):87–110, 2022.
- [28] Chun-Fu Richard Chen, Quanfu Fan, and Rameswar Panda. Crossvit: Cross-attention multi-scale vision transformer for image classification. In *Proceedings of the IEEE/CVF international conference on computer vision*, pages 357–366, 2021.
- [29] Nicolas Carion, Francisco Massa, Gabriel Synnaeve, Nicolas Usunier, Alexander Kirillov, and Sergey Zagoruyko. End-to-end object detection with transformers. In *Computer Vision–ECCV 2020: 16th European Conference, Glasgow, UK, August 23–28, 2020, Proceedings, Part I 16*, pages 213–229. Springer, 2020.
- [30] Xiaohong Huang, Zhifang Deng, Dandan Li, and Xueguang Yuan. Missformer: An effective medical image segmentation transformer. *arXiv preprint arXiv:2109.07162*, 2021.
- [31] Rafael Müller, Simon Kornblith, and Geoffrey E Hinton. When does label smoothing help? *Advances in neural information processing systems*, 32, 2019.
- [32] P. Chen, L. Gao, X. Shi, K. Allen, and L. Yang. Fully automatic knee osteoarthritis severity grading using deep neural networks with a novel ordinal loss. *Computerized Medical Imaging and Graphics*, 75:84–92, 2019.
- [33] J. Redmon and A. Farhadi. Yolo9000: better, faster, stronger. In *Proceedings of the IEEE conference on computer vision and pattern recognition*, pages 7263–7271, 2017.
- [34] Diederik P. Kingma and Jimmy Ba. Adam: A method for stochastic optimization. *CoRR*, abs/1412.6980, 2015.
- [35] A. Mikołajczyk and M. Grochowski. Data augmentation for improving deep learning in image classification problem. In *2018 International Interdisciplinary PhD Workshop (IIPhDW)*, pages 117–122, 2018.
- [36] N. V Chawla, K. W Bowyer, L. O Hall, and W P Kegelmeyer. Smote: synthetic minority over-sampling technique. *Journal of artificial intelligence research*, 16:321–357, 2002.

- [37] Ilya Loshchilov and Frank Hutter. Fixing weight decay regularization in adam, 2018.
- [38] Nitish Srivastava, Geoffrey Hinton, Alex Krizhevsky, Ilya Sutskever, and Ruslan Salakhutdinov. Dropout: a simple way to prevent neural networks from overfitting. *The journal of machine learning research*, 15(1):1929–1958, 2014.
- [39] Adam Paszke, Sam Gross, Francisco Massa, Adam Lerer, James Bradbury, Gregory Chanan, Trevor Killeen, Zeming Lin, Natalia Gimelshein, Luca Antiga, Alban Desmaison, Andreas Köpf, Edward Yang, Zach DeVito, Martin Raison, Alykhan Tejani, Sasank Chilamkurthy, Benoit Steiner, Lu Fang, Junjie Bai, and Soumith Chintala. Pytorch: An imperative style, high-performance deep learning library, 2019.
- [40] R. R. Selvaraju, M. Cogswell, A. Das, R. Vedantam, D. Parikh, and D. Batra. Grad-cam: Visual explanations from deep networks via gradient-based localization. In *2017 IEEE International Conference on Computer Vision (ICCV)*, pages 618–626, 2017.
- [41] Marta Favero, Roberta Ramonda, Mary B Goldring, Steven R Goldring, and Leonardo Punzi. Early knee osteoarthritis. *RMD open*, 1(Suppl 1):e000062, 2015.